ACS Biomaterials SCIENCE & ENGINEERING
Cite This: ACS Biomater. Sci. Eng. 2019, 5, 2926−2934
Article
pubs.acs.org/journal/abseba

Nitric Oxide Gas Delivery by Fluorinated Poly(Ethylene Glycol)@Graphene Oxide Carrier toward Pharmacotherapeutics

Yitayal Admassu Workie,[†] Sabrina,[‡] Toyoko Imae,*[,†,‡] and Marie Pierre Krafft[§]

[†]Graduate Institute of Applied Science and Technology, National Taiwan University of Science and Technology, 43 Section 4, Keelung Road, Taipei 10607, Taiwan

[‡]Department of Chemical Engineering, National Taiwan University of Science and Technology, 43 Section 4, Keelung Road, Taipei 10607, Taiwan

[§]University of Strasbourg, Charles Sadron Institute (CNRS), 23 rue du Loess, Strasbourg 67034, France

Supporting Information

ABSTRACT: In view of preparing effective nitric oxide gas carriers, a fluorinated poly(ethylene glycol) (*F*-PEG) was noncovalently conjugated with acid-treated graphene oxide (GO) to prepare the composite of *F*-PEG@GO. When the persistence of NO gas doped on GO and *F*-PEG@GO was investigated for 3 h, the conserved NO gas decreased from 49.00 ± 7.06 to 2.17 ± 1.36 nmol/mg carrier and from 58.51 ± 6.02 to 4.58 ± 2.22 nmol/mg carrier, respectively. The adsorption of *F*-PEG on GO and the doping of NO on GO and *F*-PEG@GO were declarative by the increase of distance between GO sheets, and the NO doping was also clarified by infrared absorption and X-ray photoelectron spectroscopies. The antibacterial effect was higher for NO-conserved *F*-PEG@GO than for NO-conserved GO and more effective against *Staphylococcus aureus* than against *Escherichia coli*. It is evident that the coating of *F*-PEG on GO is preferable for advancing the loading efficiency, the stability and the biomedical efficacy of NO gas.

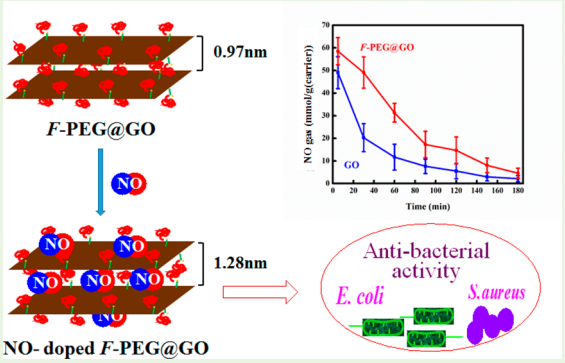

KEYWORDS: *nitric oxide, graphene oxide, fluorinated poly(ethylene glycol), antibacterial activity, Escherichia coli, Staphylococcus aureus*

INTRODUCTION

Nitric oxide (NO) is known to have vasodilator, tumoricidal and antibacterial properties.[1] However, the pharmacotherapeutic effect of NO has been limited by its concentration-dependent effect and high reactivity.[2] In response to the needs for bioactive molecules in therapy, some works have been done on the synthesis of NO donor with prodrug concept: Though several NO donors were reported like N-diazeniumdiolate,[3] S-nitrosothiol,[4] transition-metal nitrosyl complexes and alkyl nitrites,[5] there is scarce work on developing novel material that can be an efficient scaffold to store gaseous NO and deliver it to the target localization.

Graphene oxide (GO) is a sheet of carbon atoms bonded into a two-dimensional honeycomb lattice,[6] which has hydroxyl and epoxide groups at basal plane and a carboxylic acid group at its defected edges.[7] Because of the richness of oxidized functional groups, GO has the possibility of many biomedical applications, including drug delivery,[8,9] biosensing,[10] and bioimaging.[11] To increase the biocompatibility and water dispersibility, GO was hybridized with hydrophilic polymers such as polyethylene glycol,[12] sugar-based polymers,[13,14] and poly(amido amine).[9] On the other hand, fluorocarbons are excellent media of gases, in particular, of respiratory gases, because of their low intermolecular van der Waals interactions.[15] For this reason, they can be used as oxygen carriers, when they form emulsions.[16−18] Because fluorinated carbon materials may be one of the most promising carriers of gases like oxygen for biological treatments[19] but they have extremely low water dispersibility, the fluorinated carbon moiety should be hybridized with a hydrophilic moiety such as poly(ethylene glycol). Thus, the binding of fluorinated poly(ethylene glycol) (*F*-PEG) on GO will be valuable as gaseous drug delivery systems with improved biocompatibility.

In the present work, a *F*-PEG-coated GO nanocomposite platform was prepared as a novel material for NO gas delivery system. Hybridization of *F*-PEG on the surface of GO was expected to heighten the doping of the NO gas for exogenous delivery methods. The loading and self-release efficiencies of *F*-PEG@GO composites for NO gas were determined using Griess assay methods and compared with those of GO. The antibacterial activities of carried NO on GO and *F*-PEG@GO

Received: April 6, 2019
Accepted: April 22, 2019
Published: April 22, 2019

DOI: 10.1021/acsbiomaterials.9b00474
ACS Biomater. Sci. Eng. 2019, 5, 2926−2934

Scheme 1. Reactions Involved in the Formation of an Azo Dye by Coupling of Diazonium Salt of Sulfanilamide and *N*-1-Naphthylethylenediamine Dihydrochloride

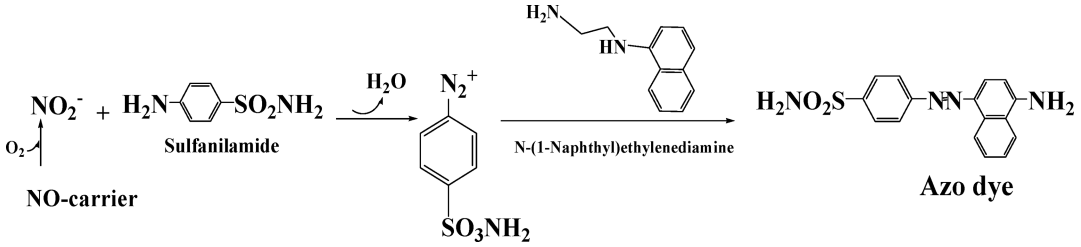

were examined against *Escherichia coli* and *Staphylococcus aureus*.

EXPERIMENTAL SECTION

Materials and Methods. Natural graphite flake of 4 μm size was obtained from Ito graphite Co. Ltd., Japan. Copper metal was purchased from Jianyuan Metal, Taiwan. Fluorinated polyethylene glycol derivative (*F*-PEG) ($F_8H_5COOPEG_{5000}$) was synthesized by esterification of F_8H_5COOH and $CH_3(OCH_2CH_2)_{5000}OH$. Other chemicals were of commercial grade. All the reagents were used as received. Ultrapure water (resistivity of 18.2 MΩ cm^{-1}, Yamato Millipore WT100) were used throughout the experimental work.

Characterization was performed using a transmission electron microscope (TEM, JEOL, Japan, 120 kV), a ultraviolet (UV)/Visible absorption spectrophotometer (UV−visible, JASCO V-670, Japan), a Fourier transform infrared absorption spectrophotometer (FTIR, NICOLET 6700, Thermo Scientific, USA), a thermogravimetric analysis (TGA, TA Q500, USA), a dynamic light scattering (DLS, SZ-100, HORIBA scientific, Japan), an X-ray diffractometer (Bruker, D2 Phaser, USA), a Raman scattering spectrometer (Horiba Jobin Yvon iHR550, Japan), a X-ray photoelectron spectrometer (XPS, VG Scientific, ESCALAB 250, England) and Brunauer−Emmett−Teller (BET) (BELSORB Max, Japan).

Preparation of *F*-PEG@GO Composites. GO sheets were prepared using the modified Hummers method from natural graphite flakes.[20] Graphite flake (2.0 g) was mixed with sulfuric acid (98%, 50 mL) under vigorous stirring at room temperature. Subsequently, sodium nitrate (2.0 g) and potassium permanganate (6.0 g) were slowly poured. The mixture was heated at 35 °C for 1 day. Water (80 mL) was added into the reacted mixture, and after the stirring was continued for 5 min, H_2O_2 (30%, 20 mL) was dropped into the reaction mixture. The product was separated from the supernatant by centrifugation (for 20 min at 6000 rpm). The precipitate was washed with an aqueous HCl solution and water until the pH of the supernatant became neutral and dried in vacuum oven overnight. For fragmentation, graphene oxides (20 mg) were ultrasonicated in water (40 mL, 0.5 mg/mL) for 4 h using a homogenizer (QSONICA Sonicator, Q700, Misonix, USA, amplitude intensity 50 and applied power 50 W) in an ice bath. The concentration of produced graphene oxide was determined from the calibration curve which was obtained by plotting the absorbance of GO at 230 nm as a function of GO concentration in water (see Figure S1). *F*-PEG@GO composites were prepared by mixing equal volumes of graphene oxide in aqueous dispersion (300 μg/mL) and *F*-PEG in aqueous solution (24 μg/mL) and sonicating for 4 h. The weight ratio of *F*-PEG:GO in *F*-PEG@GO was 0.083:1.

Quantitative Determination of Doped NO Gas by Griess Assay Method. NO gas generated by reacting aqueous nitric acid with cupper metal was continuously taken into the carrier materials (GO and *F*-PEG@GO) in the closed system. NO gas doped in carrier materials was measured using the universal Griess assay method with an affordable instrumentation and conceptually a straightforward analysis procedure.[21] As presented in the reaction Scheme 1, the principle of the measurement is the reactivity of NO in the formation of nitrite in oxygenated aqueous media[22] via the reaction with sulfanilamide under the acidic condition to form a diazonium salt intermediate. The diazonium salt intermediate is then coupled to *N*-1-naphthylethylenediamine dihydrochloride to form the stable water-soluble azo dye, which has an absorption band at λmax ≈540 nm.[23]

A stock solution of sodium nitrate (0.01 M) was prepared by dissolving sodium nitrite (17.25 mg) in water (25 mL). *N*-1-Naphthylethylenediamine dihydrochloride (25 mg) was dissolved into water (25 mL) to be a stock solution (0.1%). Sulfanilamide (250 mg, 1%) and phosphoric acid (1.25 mL, 5%) was dissolved in water (25 mL). To plot a calibration curve of sodium nitrite, we prepared a series of solutions by taking 2.25 to 11.25 μL (with an interval of 2.25 μL) from a stock solution of sodium nitrite (0.01 M) and 50 μL of both sulfanilamide and *N*-1-naphthylethylenediamine dihydrochloride and the resulting solution was further dissolved in 1.5 mL of water. The calibration curve was prepared from the absorbance of the pink-colored solution at 540 nm (see Figure S2).

The NO-doped carrier materials (10 mg) were dispersed in water (14 mL) and filtered out. For the filtrate (1 mL), 150 μL of both sulfanilamide and *N*-1-naphthylethylenediamine dihydrochloride were added. Then the nitrite concentration was determined by comparing the absorbance of the pink-colored azo dye solution at 540 nm to a calibration curve prepared with known concentrations of nitrite, and thus the amount of NO on carrier was determined stoichiometrically.

Antibacterial Activity Test. The antibacterial test was done based on the standard agar disk-diffusion method.[24] Aerobically grown *E. coli* (Gram-negative) and *S. aureus* (Gram-positive) strain suspensions (100 μL) with optical density 0.05 were spread evenly over the face of a sterile plate grown in luria bertani and tryptone soya broth agar medium, respectively. GO and *F*-PEG@GO film were prepared by homogeneously spreading their gels into a Petri dish and drying overnight. The round-shaped films of equal weight (6.25 mg) were cut out and applied as controls (non-NO doped) and tests (NO-doped) on the surface of agar plate cultured with *E. coli* and *S. aureus* by incubated for 12−16 h.

RESULTS AND DISCUSSION

Characterization of Composites. *F*-PEG@GO composite was prepared by mixing GO with *F*-PEG. TEM images were taken for GO and *F*-PEG@GO and their morphologies were compared in Figure 1: In contrast to thin GO sheets with lateral dimensions ranging around a hundred nanometers, a TEM image of *F*-PEG@GO displayed the change in morphology, suggesting the adsorption of *F*-PEG. It has been reported that the binding and covering of poly(propylene fumarate)/poly(ethyl glycol) derivative on the surface GO sheet causes to increase the size.[25] Averaged particle sizes of *F*-PEG, GO, and *F*-PEG@GO in water were measured by dynamic light scattering (Figure S3). Although the average hydrodynamic size of *F*-PEG was 1098 nm, GO and *F*-PEG@GO showed values of 207 and 250 nm, respectively. The large size of *F*-PEG indicates the aggregation of *F*-PEG. Different from such situation, when *F*-PEG was mixed with GO, the size of *F*-PEG@GO was only slightly larger than it of GO and large aggregates of *F*-PEG alone were not observed. The drastic size variation between *F*-PEG and *F*-PEG@GO suggests the

DOI: 10.1021/acsbiomaterials.9b00474
ACS Biomater. Sci. Eng. 2019, 5, 2926−2934

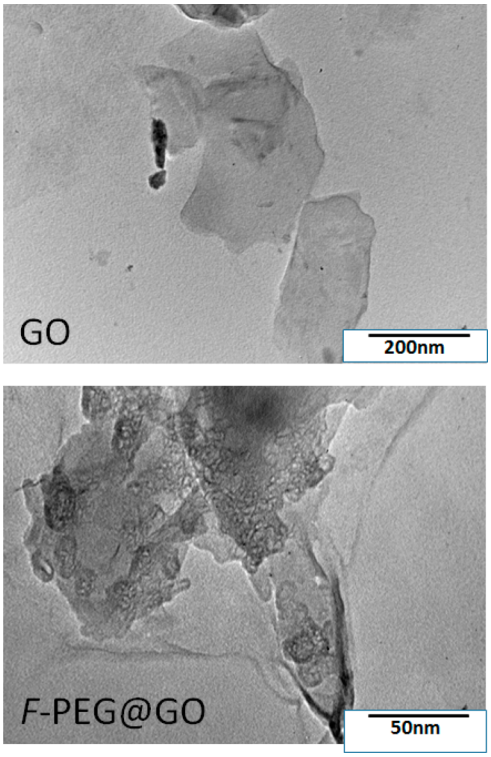

Figure 1. TEM images of GO and *F*-PEG@GO.

enough adsorption of *F*-PEG on GO and the formation of the complex.

FTIR spectra of *F*-PEG, GO and *F*-PEG@GO are shown in Figure 2A. An FTIR spectrum of *F*-PEG showed bands of O−H(H_2O) stretching (3430 cm^{-1}), alkane CH_2 stretching (2914 cm^{-1}), O−H(H_2O) bending (1640 cm^{-1}), CH_2 scissor (1460 cm^{-1}), CH_2 wagging (1350 cm^{-1}), CH_2 twisting (1258 cm^{-1}), and C−F stretching (1110 cm^{-1}). GO contains the absorption bands of O−H (3380 cm^{-1}), carbonyl C═O (1730 cm^{-1}), aromatic C═C (1630 cm^{-1}), O−H bending (1360 cm^{-1}), aromatic C−C (1220 cm^{-1}), and alkoxy C−O−C (1050 cm^{-1}) groups.[26] The appearance of oxygen-containing functional groups confirmed the preparation of GO. Meanwhile, *F*-PEG@GO composite had characteristic IR bands of both *F*-PEG and GO; CH_2 stretching (2880 cm^{-1}) and C−F stretching (1110 cm^{-1}) from *F*-PEG and carbonyl C═O (1730 cm^{-1}) from GO were noticeably observed in the composite, indicating the coexistence of *F*-PEG and GO in *F*-PEG@GO.

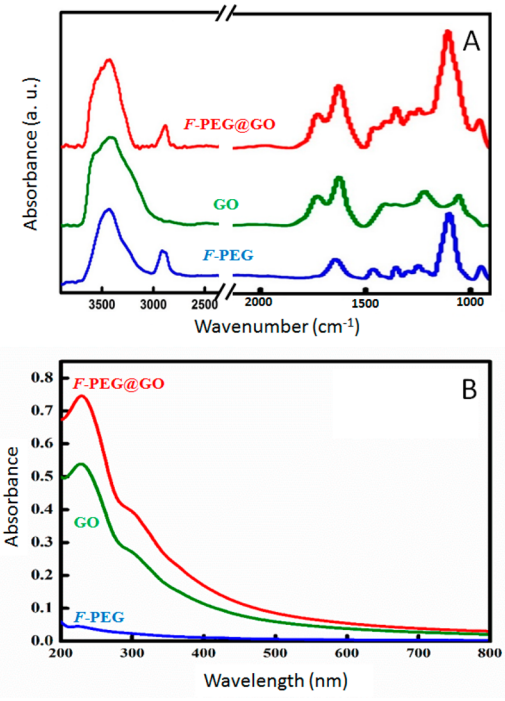

Figure 2. (A) FTIR absorption spectra of *F*-PEG, GO, and *F*-PEG@GO in KBr pellets and (B) UV−visible absorption spectra for aqueous solutions of *F*-PEG (24 mg/L), GO (75 mg/L), and *F*-PEG@GO (24:100 mg/L).

Figure 2B presents the UV−visible absorption spectra of *F*-PEG, GO, and *F*-PEG@GO. Although *F*-PEG did not show any absorption band in the region of 200 to 800 nm, GO displayed a main band at 230 nm and a shoulder band around 300 nm, which correspond to a $\pi-\pi^*$ and n-π^* electronic transition modes, respectively.[26] Same bands were observed even for *F*-PEG@GO and thus no variation happened on UV−visible absorption bands after adsorption of *F*-PEG on GO, indicating that *F*-PEG on the surface of GO does not affect the electron transition state of GO.[8]

TGA curves of GO and *F*-PEG@GO were compared as presented in Figure 3. Although graphite possessed high thermal stability in the range from 25 to 650 °C and was completely decomposed at 980 °C,[27] GO displayed 8% loss of its mass below 100 °C, because of the evaporation of adsorbed water and small molecules. The first decomposition occurred below 200 °C and lost about 29% of the mass. Additional decomposition of about 15% happened below 320 °C. The remaining mass loss (about 48%) started at 475 °C. Oxygen-including moieties should be burned in early stages and the elimination of the graphene moiety could be at the last stage but at the lower temperature than that of graphite. Thermogram of *F*-PEG@GO composite showed the thermal decomposition pattern of the 4% mass lost bellow 100 °C as a result of the evaporation of absorbed water and small molecules. The weight losses of *F*-PEG@GO happened at two steps of about 46% loss and the remaining about 50% loss. However, these losses occurred at about 27 °C higher temperature than those of GO, and the final decomposition

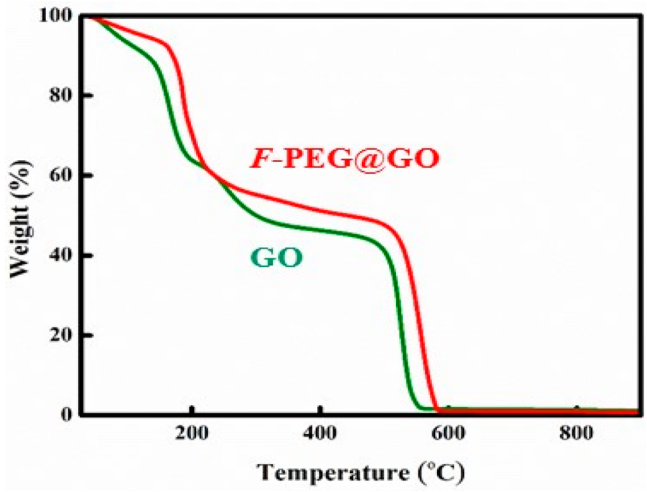

Figure 3. TGA curves of GO and *F*-PEG@GO.

DOI: 10.1021/acsbiomaterials.9b00474
ACS Biomater. Sci. Eng. 2019, 5, 2926−2934

was at 580 °C.[25] The temperature rise of the final decomposition is because of the heat-generated aromatization in *F*-PEG@GO.[28]

The XRD patterns of graphite, *F*-PEG, GO, and *F*-PEG@GO were presented in Figure 4. Although an X-ray

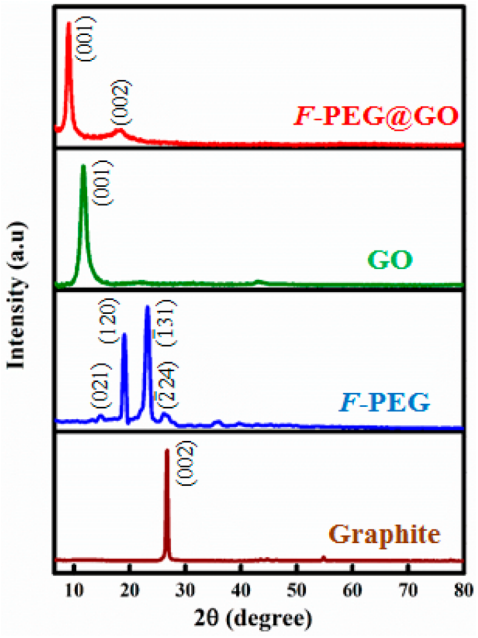

Figure 4. XRD patterns of graphite, *F*-PEG, GO, and *F*-PEG@GO.

diffractogram of graphite, the highly ordered carbon material, appeared a sharp diffraction peak (002) at 2θ = 26.60° of hexagonal crystalline structure (JPCDS No 89−8487),[27,29] an (001) peak of GO (hexagonal crystalline structure, JPCDS No 46−1628) at 11.70° confirmed the formation of graphene oxide. *F*-PEG displayed two major peaks at 19.05 and 23.30° and weak peaks at 14.69 and 26.18°, which were indexed to (120), ($\bar{1}$31), (021), and ($\bar{2}$24), respectively, of monoclinic crystalline structure (JPCDS No 52−2279).[25] However, the addition of *F*-PEG on GO arose a strong peak to diffract at 9.14° and a weak peak at 18.40° assigned to (001) and (002), respectively, of hexagonal crystalline structure (JPCDS No 53−1791), although the composite pattern does not show apparent Bragg peaks from *F*-PEG because of the relatively weak Bragg peaks of *F*-PEG in comparison with those of GO.[30] These results indicate the strong adsorption of *F*-PEG on GO enough to perturb the crystallography of each component.

Figure 5 presents the Raman spectra of graphite, *F*-PEG, GO, and *F*-PEG@GO. For *F*-PEG, bands appeared at 2936 cm^{-1} was assigned to stretching vibration mode of alkyl chain. The CH_2 scissoring, wagging and twisting bands were found at 1471, 1271, and 1225 cm^{-1}, respectively. A band at 1132 cm^{-1} attributed to C−F stretching mode and the C−O−C stretching vibration band was observed at 1055 cm^{-1}. A band at 835 cm^{-1} was assigned to carbon skeleton of *F*-PEG.[31] Graphite had three Raman bands: A G-band (sp^2) and a weak D-band (sp^3) appeared at 1581 and 1326 cm^{-1}, respectively, and a 2D band was observed at 2689 cm^{-1}.[32] In GO, the appearance of a D-band at 1351 cm^{-1} besides a G-band at 1583 cm^{-1} confirms the partial defect of graphitic structure in GO. The G-band and D-band (1578 and 1342 cm^{-1}, respectively) of *F*-PEG@GO were scarcely changed, as

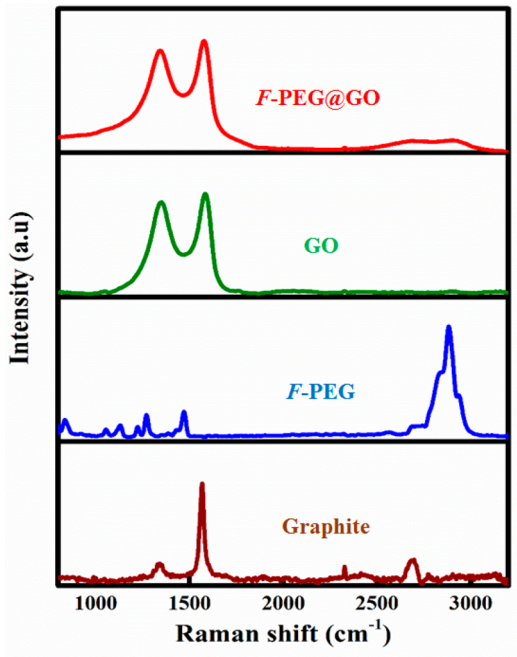

Figure 5. Raman spectra of graphite, *F*-PEG, GO, and *F*-PEG@GO.

compared to GO,[33] and the alky chain vibration bands of *F*-PEG around 2936 cm^{-1} were weak. Noncovalent binding of *F*-PEG on GO may cause the scarce variation on the vibration state.

Doping of NO Gas. The loading efficiency of NO in carriers was evaluated. The loaded amount of NO after 5 min was 58.51 ± 6.02 mmol/g for *F*-PEG@GO carrier and 49.00 ± 7.06 mmol/g for GO carrier. However, the loaded NO in both carriers decreased with time in air atmosphere and thus it came down to 4.58 ± 2.22 and 2.17 ± 1.36 mmol/g(carrier), respectively, after 3 h, as seen in Figure 6. This phenomenon may happen by the reasons that NO was probably oxidized to NO_2 by coexisting oxygen or released from the carrier. Thus, it was confirmed that GO can load NO but the coating of *F*-PEG on the surface of GO enhanced the trapping ability of NO gas

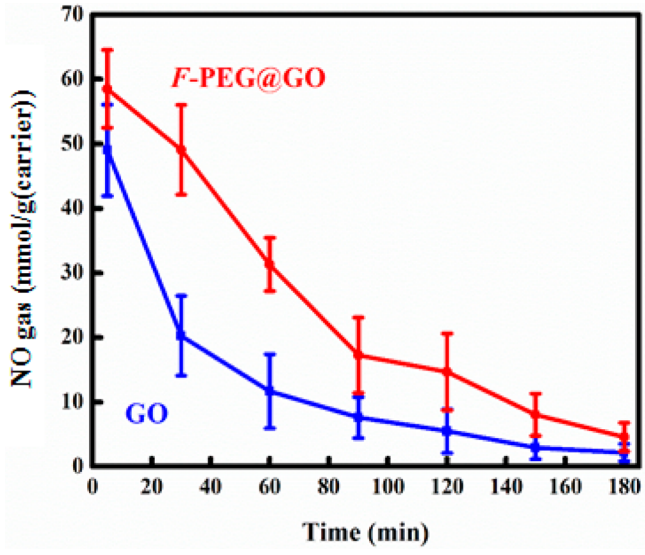

Figure 6. NO gas reserved in GO and *F*-PEG@GO carriers.

DOI: 10.1021/acsbiomaterials.9b00474
ACS Biomater. Sci. Eng. 2019, 5, 2926−2934

on the carrier. Moreover, the reservation of NO gas on carriers was only 8% for *F*-PEG@GO and 4% for GO.

Nitrogen adsorption−desorption isotherms at 77 K were measured for GO and *F*-PEG@GO. The isotherms and BET parameters are shown in Figure 7 and Table 1, respectively.

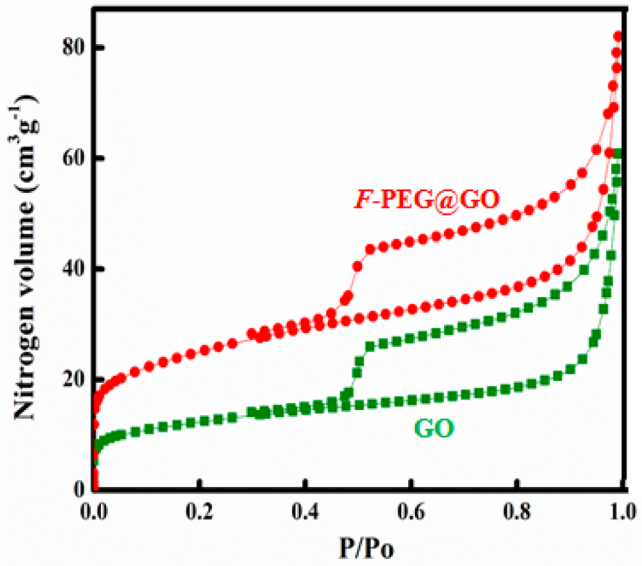

Figure 7. Nitrogen adsorption−desorption isotherm of GO and *F*-PEG@GO at 77 K.

Table 1. Analytical Results of Adsorption-Desorption Isotherms of GO and *F*-PEG@GO

nanomaterial	specific surface area (m^2/g)	pore volume (cm^3/g)	mean pore diameter (nm)
GO	42.88	0.088	8.28
F-PEG@GO	86.97	0.122	5.59

The physical adsorption isotherms of both GO and *F*-PEG@GO were classified as IV. The specific surface area and pore volume of *F*-PEG@GO were higher than those of GO because of the binding by *F*-PEG, although the mean pore diameter was lowered after the binding of *F*-PEG. Analytical results of isotherms indicate that the NO gas doping of GO and *F*-PEG@GO may depend on their surface area and pore volume.

After NO gas was doped on GO and *F*-PEG@GO, FTIR absorption spectra were compared with those of carriers before NO doping. As seen in Figure 8A(a b), even after NO was doped, intrinsic absorption bands of both GO and *F*-PEG@GO were conserved, except the appearance of a strong band at 1384 cm^{-1}, which may be attributed to a NO-related vibration mode. This result confirmed the proper loading of NO in GO and *F*-PEG@GO carriers. Figure 8A(c) displays FTIR absorption spectra of GO, which was NO-doped and left without additional doping for an adequate time, as indicated in the figure. A band at 1384 cm^{-1} decreased and the diminution was calculated as an intensity ratio of a band at 1384 cm^{-1} against the intensity of a band at 1630 cm^{-1}, where a band intensity at 1384 cm^{-1} was subtracted the contribution of intrinsic GO band. The ratio of 2.4 at 10 min decreased to 1.4 after 120 min. This tendency is consistent with the decrease in NO in Figure 6.

The effect of NO doping on the crystalline structure of GO and *F*-PEG@GO was also investigated as presented in Figure 8B. The (001) diffraction peak of GO was shifted to low angle by 3.50° from its intrinsic peak position (11.70°) as a result of NO doping. The (001) peak of *F*-PEG@GO was similarly changed from 9.14 to 6.85°, which is a decrease of 2.29°. These shifts of (001) peaks correspond to 0.32 and 0.31 nm expansion of hexagonal layers after NO doping in GO and *F*-PEG@GO, respectively. Considering to the space size (0.76 nm) between GO sheets, the space size (0.97 nm) after adsorption of *F*-PEG, and the molecular size (0.39 nm × 0.28 nm) of NO, the structures of GO, *F*-PEG@GO, and their NO-doping states can be estimated as illustrated in Scheme 2. It is

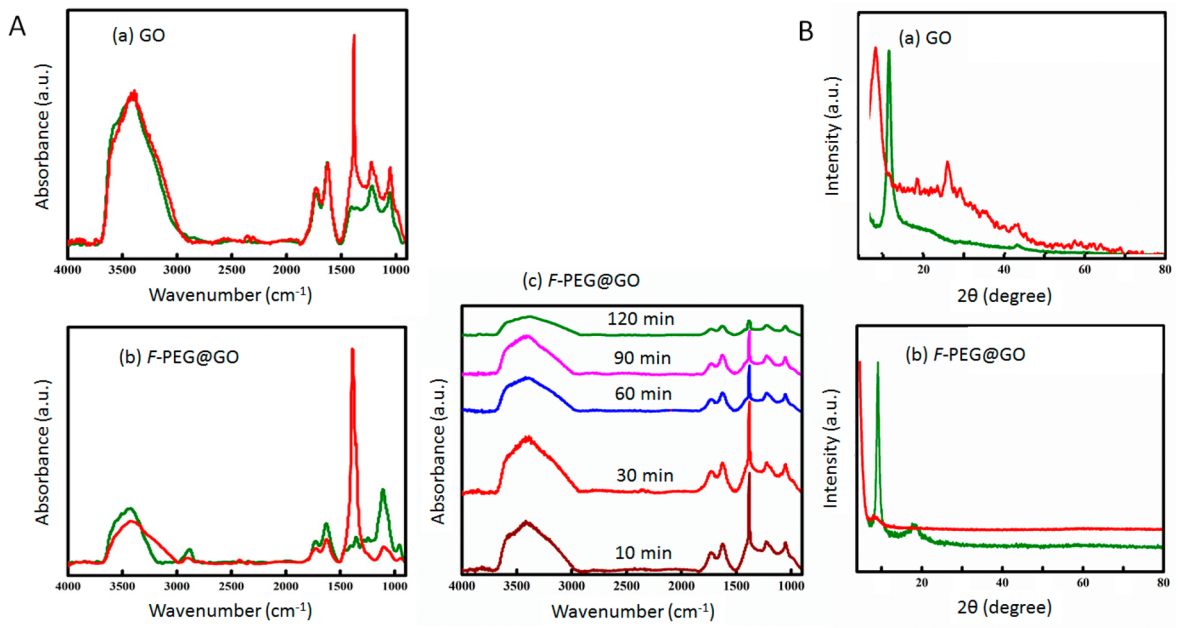

Figure 8. (A) FTIR absorption spectra and (B) XRD patterns of (a) GO and (b) *F*-PEG@GO. Green, NO-non-doped; red, NO-doped. (A)(c) Time dependence of FTIR absorption spectra of NO-doped GO. Time indicates after NO doping.

DOI: 10.1021/acsbiomaterials.9b00474
ACS Biomater. Sci. Eng. 2019, 5, 2926−2934

Scheme 2. Schematic Illustration of Adsorption of *F*-PEG on GO and NO Doping on GO and *F*-PEG@GO

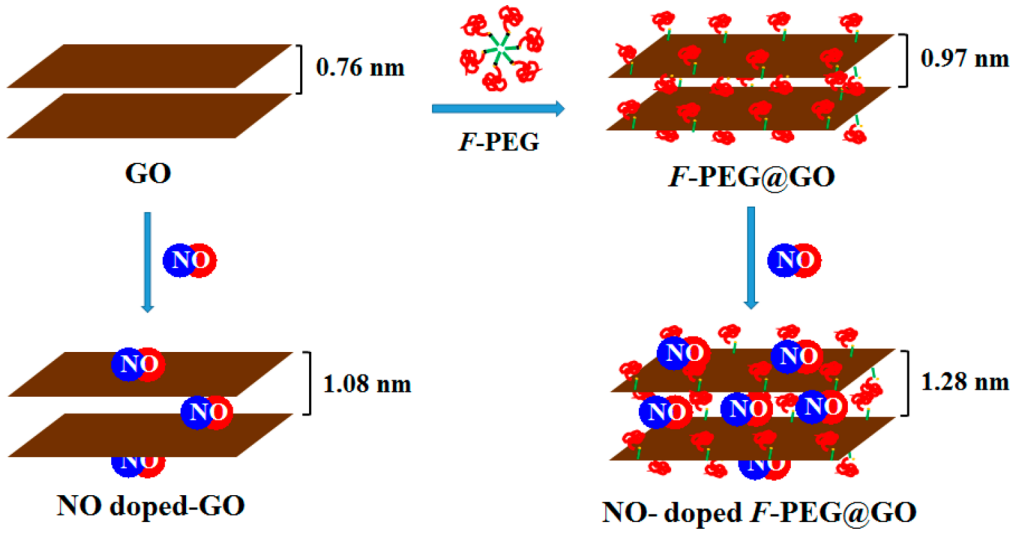

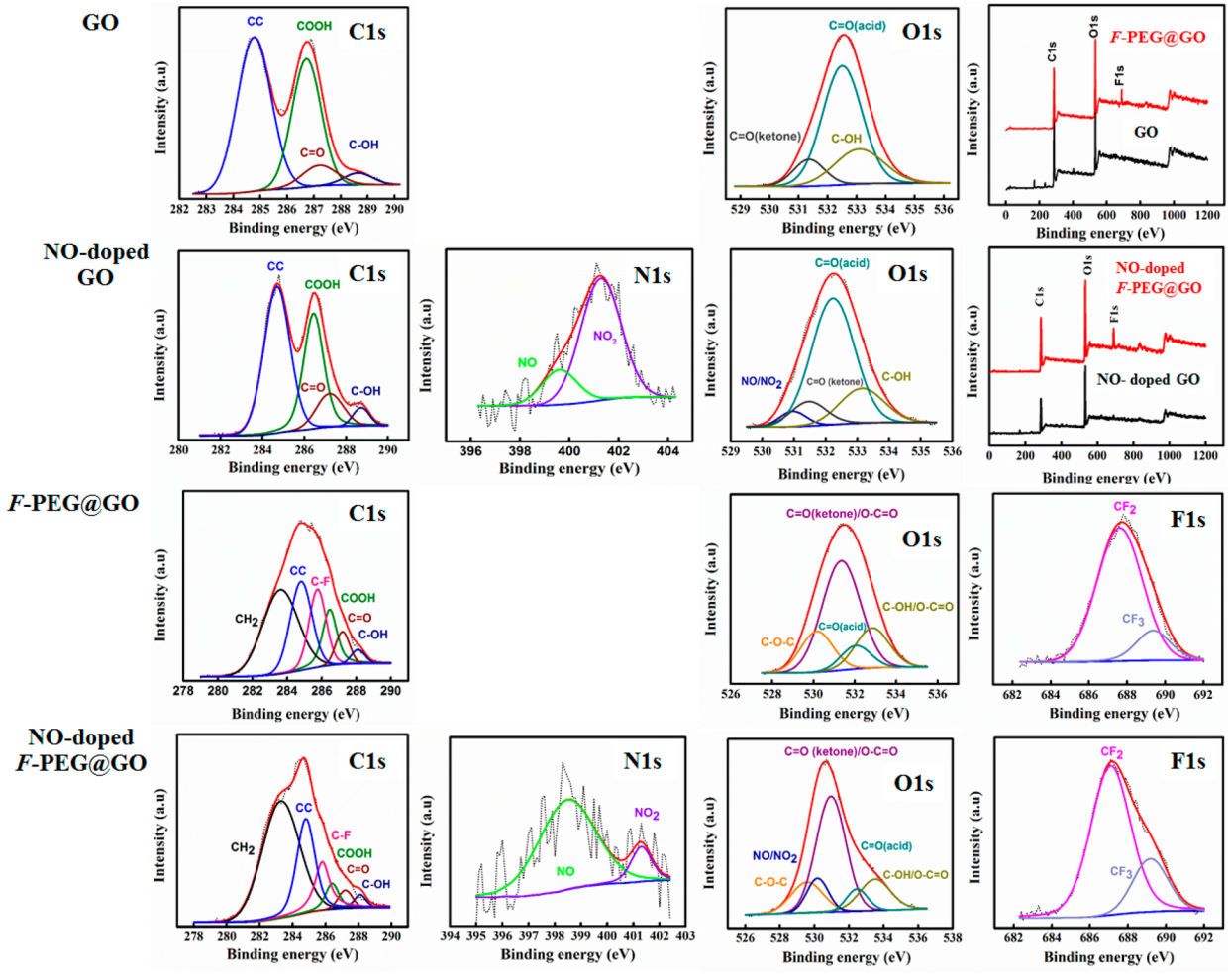

Figure 9. XPS spectra and elemental deconvolution spectra of GO, *F*-PEG@GO, NO-doped GO, and NO-doped *F*-PEG@GO.

clearly shown that the crystalline structure of GO and *F*-PEG@GO expanded because of the adsorption-induced deformation effect of NO gas.

The variation of chemical composition in GO and *F*-PEG@GO before and after NO doping was assessed using XPS as shown in Figure 9, where full XPS scan and fine analyses including their deconvolution are presented. The binding energy and the area intensity of deconvoluted peaks are given in Table 2. Full XPS scan surveys were exhibited peaks that are assigned to C 1s, N 1s, O 1s, and F 1s. GO possessed deconvoluted C 1s species of aromatic CC, carboxylic acid (COOH), ketone (C═O) and hydroxyl (C−OH).[6,34] *F*-

DOI: 10.1021/acsbiomaterials.9b00474
ACS Biomater. Sci. Eng. 2019, 5, 2926−2934

Table 2. Binding Energy and Area Intensity from XPS Spectra of GO, *F*-PEG@GO, NO-Doped GO, and NO-Doped *F*-PEG@GO

	GO		NO-doped GO		*F*-PEG@GO		NO-doped *F*-PEG@GO		
element	BE (eV)	area intensity	BE (eV)	area intensity	BE (eV)	area intensity	BE (eV)	area intensity	assignment
					283.6	1735	283.6	2588	CH_2[a]
C 1s	284.8	3463	284.8	1494	284.8	1120	284.8	1168	CC (aromatic)
					285.8	810	285.8	608	CF[a]
	286.7	2448	286.7	997	286.4	575	286.4	253	COOH (acid)
	287.2	472	287.2	342	287.2	262	287.2	148	C═O (ketone)
	288.7	219	288.7	114	288.1	110	2881.	103	COH (hydroxyl)
N 1s			399.5	30			399.5	64	NO[b]
			401.2	117			401.3	10	NO_2[b]
O 1s					530.1	1010	529.6	996	COC (ether)[a]
			530.9	200			530.3	479	NO[b], NO_2[b]
	531.4	991	531.4	448	531.4	3144	531.0	3540	C═O (ketone) O−C═O (ester)[a]
	532.5	5433	532.5	2632	532.1	520	532.4	475	C═O (acid)
	533.1	1944	533.1	762	532.8	1033	533.5	1062	COH (acid, hydroxyl) O−C═O (ester)[a]
F 1s					687.7	882	687.1	1509	CF_2[a]
					689.3	167	689.2	428	CF_3[a]

[a]Assignment to *F*-PEG. [b]Assignment to NO or NO_2.

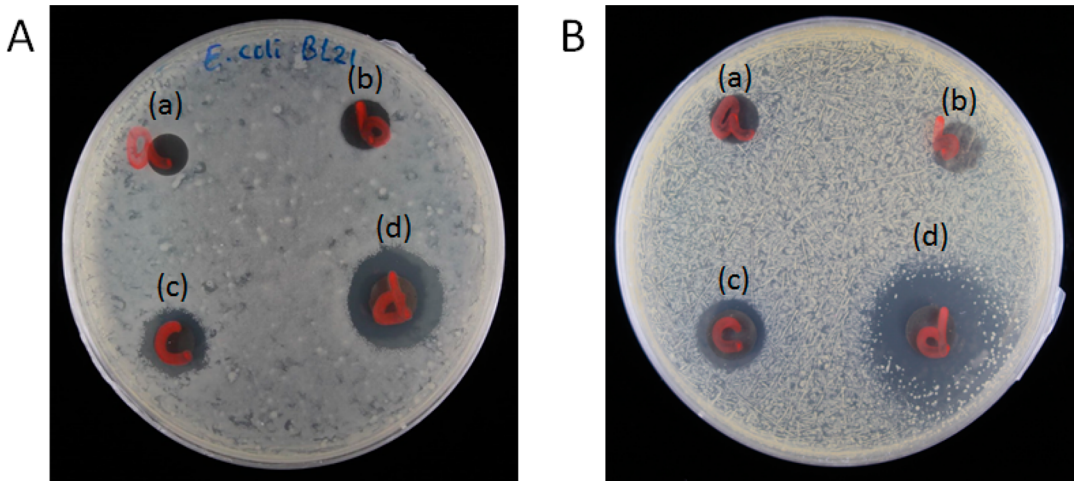

Figure 10. Images after antibacterial test for (A) *E. coli* and (B) *S. aureus* on (a) control GO, (b) control *F*-PEG@GO (c) NO-doped GO, and (d) NO-doped *F*-PEG@GO.

PEG@GO showed additional alkyl (CH_2) and carbon−fluorine (C−F) species contributed from *F*-PEG.[35] O 1s fine analysis appeared chemical species of ketone (C═O), carboxylic acid (C═O and OH) and hydroxyl (OH) in GO.[36] On the other hand, *F*-PEG@GO showed an additional species of ether (COC) from *F*-PEG but the binding energies of ester (C═O and C−O) overlapped on binding energies of species from GO. Another characteristic of *F*-PEG@GO different from GO is that the existence of F 1s originated from CF_2 and CF_3 in *F*-PEG. The existence of these species is consistent with the results from FTIR and Raman spectra.

Essentially, similar binding energies and area intensities were obtained for species of GO besides additional species from *F*-PEG even after the binding of *F*-PEG and, moreover, the binding species and their energies of GO and *F*-PEG@GO were not significantly changed after NO doping. These results imply that the chemical state of GO was not affected by noncovalent functionalization by *F*-PEG, coinciding with the result of the electronic state from UV−visible absorption spectra.

It should be noted that both NO-doped GO and *F*-PEG@GO provided chemical species of both NO and NO_2: N 1s fine analysis of GO and *F*-PEG@GO showed two species coming from NO[37] and NO_2,[38] although O 1s of NO and NO_2 indicated similar binding energies. Relatively higher area intensity of NO species in N 1s of *F*-PEG@GO than those of NO_2 species in N 1s of *F*-PEG@GO and NO species in N 1s of GO may support the result of NO loading in *F*-PEG@GO superior to GO as shown in Figure 6. Coexisting NO_2 may be doped simultaneously with NO or oxidized from NO.

Antibacterial Effect of NO Doped on GO and *F*-PEG@GO. Following the reports that NO is known as a promising antibacterial agent,[39] the in vitro antibacterial activity of NO in GO and *F*-PEG@GO carriers was examined against Gram-negative and Gram-positive bacteria compared to control, as presented in Figure 10. Although the grown *E. coli* colonies were clearly visible on the control GO, the NO-doped GO showed antibacterial activity toward *E. coli* (see Figure 10A(a, c)) with an 11.5 mm diameter zone of inhibition. Similarly, the growth of *E. coli* colonies occurred on the control of *F*-PEG@GO but NO-doped *F*-PEG@GO displayed significant

DOI: 10.1021/acsbiomaterials.9b00474
ACS Biomater. Sci. Eng. 2019, 5, 2926−2934

antibacterial activity against *E. coli* with a wider zone of inhibition (18.2 mm in diameter) than N-doped GO (see Figure 10A(b, d)). The same tendency was observed even for *S. aureus*. As shown in Figure 10B, control GO did not influence the growth of *S. aureus*, but the doping of NO on GO inhibited its growth by 13.3 mm diameter (Figure 10B(a, c)). Correspondingly, although control *F*-PEG@GO had no resistance on the growth of bacteria, NO-doped *F*-PEG@GO showed the observable conquest against pathogen with the higher zone of inhibition (24.8 mm in diameter) than NO-doped GO (Figure 10B(b, d)). Moreover, it should be noted that NO was more effective for *S. aureus* than for *E. coli*. A similar result was reported previously.[40] NO loading systems in the present work with antibacterial activity without chemical derivatization showed a comparable conservation efficiency to the previously reported NO donors, N-diazeniumdiolate and S-nitrosothiol, with a principle of chemical variation in the carrier.[41] The in vivo antibacterial activity of NO donors with the prodrug concept was reported on mice.[42,43] NO released from the donors was applied for healing of acute and chronic wounds. NO-gas-loaded carrier in the present work, potentially active as an antimicrobial agent, should then act even in the wound healing of mice.

CONCLUSIONS

The biomedical application of NO is limited because of the instability of the gas and the unavailability of the materials that were developed to encapsulate the gas. In this work, a NO-preserving graphene-based platform and its composite with *F*-PEG were successfully prepared. The conserving efficiencies of the GO and *F*-PEG@GO were compared on the same time course framework. The efficiency may depend on the chemical structure and characteristics of NO carriers. Graphene was assumed to be familiar to NO doping. However, as the GO does not show high porosity, using other porous solids will enhance the NO adsorption. Another possible trial to increasing the NO conservation is the creation of the hydrophobic domain possessing gas-encapsulating properties. Thus, the *F*-PEG-coated GO composite with hydrophobic perfluorocarbon moiety was effective for NO conservation superior to GO. Moreover, *F*-PEG@GO exerted more of an antibacterial effect than did GO. However, the NO conservation on these carriers showed a decreasing tendency with time. This phenomenon should be the oxidation of NO to NO_2 rather than the release of NO from the carrier. Thus, further invention is necessary to creating a conserved NO-protecting system.

ASSOCIATED CONTENT

Supporting Information

The Supporting Information is available free of charge on the ACS Publications website at DOI: 10.1021/acsbiomaterials.9b00474.

UV−visible absorption spectra of commercial GO at 100−500 mg/L and a calibration curve of GO obtained from absorbance at 230 nm/UV−visible absorption spectra of azo dye at 15−75 μM and a calibration curve of azo dye obtained from absorbance at 540 nm/ Histograms of particle size distribution of *F*-PEG, GO and *F*-PEG@GO (PDF)

AUTHOR INFORMATION

Corresponding Author

*E-mail: imae@mail.ntust.edu.tw (T.I.). Tel.: +886227303627.

ORCID

Toyoko Imae: 0000-0003-2731-1960

Notes

The authors declare no competing financial interest.

ACKNOWLEDGMENTS

This work was partially supported by a grant from the France/Taiwan Programme of Integrated Actions (PIA) Orchid. YAW gratefully acknowledge National Taiwan University of Science and Technology, Taiwan, for the financial support by a student scholarship. Authors also thank to Prof. C. K. Lee and Prof. M. Ujihara, National Taiwan University of Science and Technology, Taiwan, and Prof. Mounir Tarek, CNRS, France, for their valuable discussion and support. Authors also give a thank to Dr. M. M. M. Ahmed, Dr. C.-C. Chang, and Mr. J.-Y. Rao, National Taiwan University of Science and Technology, Taiwan, for their kind technical support.

REFERENCES

(1) Shin, J. H.; Metzger, S. K.; Schoenfisch, M. H. Synthesis of Nitric Oxide-Releasing Silica Nanoparticles. *J. Am. Chem. Soc.* **2007**, *129*, 4612−4619.

(2) Friedman, A. J.; Han, G.; Navati, M. S.; Chacko, M.; Gunther, L.; Alfieri, A.; Friedman, J. M. Sustained release nitric oxide releasing nanoparticles: characterization of a novel delivery platform based on nitrite containing hydrogel/glass composites. *Nitric Oxide* **2008**, *19* (1), 12−20.

(3) Chakrapani, H.; Maciag, A. E.; Citro, M. L.; Keefer, L. K.; Saavedra, J. E. Cell-Permeable Esters of Diazeniumdiolate-Based Nitric Oxide Prodrugs. *Org. Lett.* **2008**, *10* (22), 5155−5158.

(4) Lutzke, A.; Tapia, J. B.; Neufeld, M. J.; Reynolds, M. M. Sustained Nitric Oxide Release from a Tertiary S-Nitrosothiol-based Polyphosphazene Coating. *ACS Appl. Mater. Interfaces* **2017**, *9* (3), 2104−2113.

(5) Luo, R.; Liu, Y.; Yao, H.; Jiang, L.; Wang, J.; Weng, Y.; Zhao, A.; Huang, N. Copper-Incorporated Collagen/Catechol Film for in Situ Generation of Nitric Oxide. *ACS Biomater. Sci. Eng.* **2015**, *1* (9), 771−779.

(6) Yu, H.; Zhang, B.; Bulin, C.; Li, R.; Xing, R. High-efficient Synthesis of Graphene Oxide Based on Improved Hummers Method. *Sci. Rep.* **2016**, *6*, 36143.

(7) Gao, W.; Alemany, L. B.; Ci, L.; Ajayan, P. M. New insights into the structure and reduction of graphite oxide. *Nat. Chem.* **2009**, *1* (5), 403−408.

(8) Chen, J.; Liu, H.; Zhao, C.; Qin, G.; Xi, G.; Li, T.; Wang, X.; Chen, T. One-step reduction and PEGylation of graphene oxide for photothermally controlled drug delivery. *Biomaterials* **2014**, *35* (18), 4986−95.

(9) Siriviriyanun, A.; Popova, M.; Imae, T.; Kiew, L. V.; Looi, C. Y.; Wong, W. F.; Lee, H. B.; Chung, L. Y. Preparation of graphene oxide/dendrimer hybrid carriers for delivery of doxorubicin. *Chem. Eng. J.* **2015**, *281*, 771−781.

(10) Georgakilas, V.; Tiwari, J. N.; Kemp, K. C.; Perman, J. A.; Bourlinos, A. B.; Kim, K. S.; Zboril, R. Noncovalent Functionalization of Graphene and Graphene Oxide for Energy Materials, Biosensing, Catalytic, and Biomedical Applications. *Chem. Rev.* **2016**, *116* (9), 5464−519.

(11) Nanda, S. S.; Papaefthymiou, G. C.; Yi, D. K. Functionalization of Graphene Oxide and its Biomedical Applications. *Crit. Rev. Solid State Mater. Sci.* **2015**, *40* (5), 291−315.

(12) Kiew, S. F.; Kiew, L. V.; Lee, H. B.; Imae, T.; Chung, L. Y. Assessing biocompatibility of graphene oxide-based nanocarriers: A review. *J. Controlled Release* **2016**, *226*, 217−228.

DOI: 10.1021/acsbiomaterials.9b00474
ACS Biomater. Sci. Eng. 2019, 5, 2926−2934

(13) Hsu, Y. H.; Hsieh, H. L.; Viswanathan, G.; Voon, S. H.; Kue, C. S.; Saw, W. S.; Yeong, C. H.; Azlan, C. A.; Imae, T.; Kiew, L. V.; Lee, H. B.; Chung, L. Y. Multifunctional carbon-coated magnetic sensing graphene oxide-cyclodextrin nanohybrid for potential cancer theranosis. *J. Nanopart. Res.* **2017**, *19* (11), 359−378.
(14) Kiew, S. F.; Ho, Y. T.; Kiew, L. V.; Kah, J. C. Y.; Lee, H. B.; Imae, T.; Chung, L. Y. Preparation and characterization of an amylase-triggered dextrin-linked graphene oxide anticancer drug nanocarrier and its vascular permeability. *Int. J. Pharm.* **2017**, *534* (1−2), 297−307.
(15) Krafft, M. P.; Riess, J. G. Perfluorocarbons, life sciences and biomedical uses. *J. Polym. Sci., Part A: Polym. Chem.* **2007**, *45*, 1185−1198.
(16) Krafft, M. Fluorocarbons and fluorinated amphiphiles in drug delivery and biomedical research. *Adv. Drug Delivery Rev.* **2001**, *47*, 209−228.
(17) Riess, J. G. Injectable oxygen carriers (blood substitutes) - Raison d'être, chemistry, and some physiology. *Chem. Rev.* **2001**, *101*, 2797−2920.
(18) Haiss, F.; Jolivet, R.; Wyss, M. T.; Reichold, J.; Braham, N. B.; Scheffold, F.; Krafft, M. P.; Weber, B. Improved *in vivo* two-photon imaging after blood replacement by perfluorocarbon. *J. Physiol.* **2009**, *587*, 3153−3158.
(19) Maio, A.; Scaffaro, R.; Lentini, L.; Piccionello, A. P.; Pibiri, I. Perfluorocarbons−graphene oxide nanoplatforms as biocompatible oxygen reservoirs. *Chem. Eng. J.* **2018**, *334*, 54−65.
(20) Sun, L.; Wang, L.; Tian, C.; Tan, T.; Xie, Y.; Shi, K.; Li, M.; Fu, H. Nitrogen-doped graphene with high nitrogen level via a one-step hydrothermal reaction of graphene oxide with urea for superior capacitive energy storage. *RSC Adv.* **2012**, *2* (10), 4498−4506.
(21) Hetrick, E. M.; Schoenfisch, M. H. Analytical chemistry of nitric oxide. *Annu. Rev. Anal. Chem.* **2009**, *2*, 409−33.
(22) Ignarro, L. J.; Fukuto, J. M.; Griscavage, J. M.; Rogers, N. E.; Byrns, R. E. Oxidation of nitric oxide in aqueous solution to nitrite but not nitrate: Comparison with enzymatically formed nitric oxide from L-arginine. *Proc. Natl. Acad. Sci. U. S. A.* **1993**, *90*, 8103−8107.
(23) Nims, R. W.; Darbyshire, J. F.; Saavedra, J. E.; Christodoulou, D.; Hanbauer, I.; Cox, G. W.; Grisham, M. B.; Laval, F.; Cook, J. A.; Krishna, M. C.; Wink, D. A. Colorimeteric methods for the determination of Nitric oxide concentration in neutral aqueous solutions. *Methods* **1995**, *7*, 48−54.
(24) Balouiri, M.; Sadiki, M.; Ibnsouda, S. K. Methods for in vitro evaluating antimicrobial activity: A review. *J. Pharm. Anal.* **2016**, *6* (2), 71−79.
(25) Diez-Pascual, A. M.; Diez-Vicente, A. L. Poly(propylene fumarate)/Polyethylene Glycol-Modified Graphene Oxide Nanocomposites for Tissue Engineering. *ACS Appl. Mater. Interfaces* **2016**, *8* (28), 17902−14.
(26) Siriviriyanun, A.; Imae, T.; Calderó, G.; Solans, C. Photo-therapeutic functionality of biocompatible graphene oxide/dendrimer hybrids. *Colloids Surf., B* **2014**, *121*, 469−473.
(27) Ujihara, M.; Ahmed, M. M. M.; Imae, T.; Yamauchi, Y. Massive-exfoliation of magnetic graphene fromacceptor-type GIC by long-chain alkyl amine. *J. Mater. Chem. A* **2014**, *2*, 4244−4250.
(28) Kebede, M. A.; Imae, T.; Sabrina; Wu, C. M.; Cheng, K. B. Cellulose fibers functionalized by metal nanoparticles stabilized in dendrimer for formaldehyde decomposition and antimicrobial activity. *Chem. Eng. J.* **2017**, *311*, 340−347.
(29) Paulchamy, B.; Arthi, G.; Lignesh, B. D. A Simple Approach to Stepwise Synthesis of Graphene Oxide Nanomaterial. *J. Nanomed. Nanotechnol.* **2015**, *06* (01), 1−4.
(30) Wang, C.; Feng, L.; Yang, H.; Xin, G.; Li, W.; Zheng, J.; Tian, W.; Li, X. Graphene oxide stabilized polyethylene glycol for heat storage. *Phys. Chem. Chem. Phys.* **2012**, *14* (38), 13233−8.
(31) León, A.; Reuquen, P.; Garín, C.; Segura, R.; Vargas, P.; Zapata, P.; Orihuela, P. A. FTIR and Raman Characterization of TiO_2 Nanoparticles Coated with Polyethylene Glycol as Carrier for 2-Methoxyestradiol. *Appl. Sci.* **2017**, *7* (12), 49−58.
(32) Kudin, K. N.; Ozbas, B.; Schniepp, H. C.; Prud'homme, R. K.; Aksay, I. A.; Car, R. Raman Spectra of Graphite Oxide and Functionalized Graphene Sheets. *Nano Lett.* **2008**, *8*, 36−41.
(33) Yamini, D.; Venkatasubbu, G. D.; Kumar, J.; Ramakrishnan, V. Raman scattering studies on PEG functionalized hydroxyapatite nanoparticles. *Spectrochim. Acta. A Mol. Biomol. Spectrosc.* **2014**, *117*, 299−303.
(34) Efa, M. T.; Imae, T. Hybridization of carbon-dots with ZnO nanoparticles of different sizes. *J. Taiwan Inst. Chem. Eng.* **2018**, *92*, 112−117.
(35) Jankovský, O.; Simek, P.; Sedmidubsky, D.; Matejkova, S.; Janousek, Z.; Sembera, F.; Pumera, M.; Sofer, Z. Water-soluble highly fluorinated graphite oxide. *RSC Adv.* **2014**, *4* (3), 1378−1387.
(36) Yu, B.; Wang, X.; Qian, X.; Xing, W.; Yang, H.; Ma, L.; Lin, Y.; Jiang, S.; Song, L.; Hu, Y.; Lob, S. Functionalized graphene oxide/phosphoramide oligomer hybrids flame retardant prepared via in situ polymerization for improving the fire safety of polypropylene. *RSC Adv.* **2014**, *4*, 31782−31794.
(37) Bukhtiyarov, A. V.; Kvon, R. I.; Nartova, A. V.; Prosvirin, I. P.; Bukhtiyarov, V. I. In-situ XPS investigation of nitric oxide adsorption on (111), (310), and (533) gold single crystal faces. *Surf. Sci.* **2012**, *606* (3−4), 559−563.
(38) Ranke, W. UPS and XPS reference data of O, N, NO, $(NO_2)_2$, NH_3, H_2O, OH, H_2S, SH and S on Ge surfaces. *J. Electron Spectrosc. Relat. Phenom.* **1993**, *61*, 231−240.
(39) Schairer, D. O.; Chouake, J. S.; Nosanchuk, J. D.; Friedman, A. J. The potential of nitric oxide releasing therapies as antimicrobial agents. *Virulence* **2012**, *3* (3), 271−9.
(40) Cardozo, V. F.; Lancheros, C. A. C.; Narciso, A. M.; Valereto, E. C. S.; Kobayashi, R. K. T.; Seabra, A. B.; Nakazato, G. Evaluation of antibacterial activity of nitric oxide-releasing polymeric particles against Staphylococcus aureus and Escherichia coli from bovine mastitis. *Int. J. Pharm.* **2014**, *473* (1−2), 20−9.
(41) Hetrick, E. M.; Shin, J. H.; Stasko, N. A.; Johnson, C. B.; Wespe, D. A.; Holmuhamedov, E.; Schoenfisch, M. H. Bactericidal Efficacy of Nitric Oxide-Releasing Silica Nanoparticles. *ACS Nano* **2008**, *2*, 235−246.
(42) Martinez, L. R.; Han, G.; Chacko, M.; Mihu, M. R.; Jacobson, M.; Gialanella, P.; Friedman, A. J.; Nosanchuk, J. D.; Friedman, M. J. Antimicrobial and healing efficacy of sustained release Nitric Oxide nanoparticles against staphylococcus aureus skin infection. *J. Invest. Dermatol.* **2009**, *129*, 2463−2469.
(43) Neidrauer, M.; Ercan, U. K.; Bhattacharyya, A.; Samuels, J.; Sedlak, J.; Trikha, R.; Barbee, K. A.; Weingarten, M. S.; Joshi, S. G. Antimicrobial efficacy and wound-healing property of a topical ointment containing nitric-oxide-loaded zeolites. *J. Med. Microbiol.* **2014**, *63*, 203−209.

DOI: 10.1021/acsbiomaterials.9b00474
ACS Biomater. Sci. Eng. 2019, 5, 2926−2934